Eur. J. Mineral.
2017, **29**, 923–930
Published online 26 June 2017

Wilancookite, $(Ba,K,Na)_8(Ba,Li,\square)_6Be_{24}P_{24}O_{96}\cdot 32H_2O$, a new beryllophosphate with a zeolite framework

FRÉDÉRIC HATERT[1,*], SIMON PHILIPPO[2], LUISA OTTOLINI[3], FABRICE DAL BO[1], RICARDO SCHOLZ[4], MÁRIO L.S.C. CHAVES[5], HEXIONG YANG[6], ROBERT T. DOWNS[6] and LUIZ A.D. MENEZES FILHO[7,a]

[1] Laboratoire de Minéralogie, Université de Liège B18, 4000 Liège, Belgium
*Corresponding author, e-mail: fhatert@ulg.ac.be
[2] Section Minéralogie, Musée National d'Histoire Naturelle, Rue Münster 25, 2160 Luxembourg City, Luxembourg
[3] C.N.R. – Istituto di Geoscienze e Georisorse (IGG), Unità di Pavia, Via A. Ferrata 1, 27100 Pavia, Italy
[4] Universidade Federal de Ouro Preto (UFOP), Escola de Minas, Departamento de Geologia, Campus Morro do Cruzeiro, 35400-000 Ouro Preto, MG, Brazil
[5] Universidade Federal de Minas Gerais (UFMG), Instituto de Geociências, Avenida Antônio Carlos, 6627, 31270-902 Belo Horizonte, MG, Brazil
[6] Department of Geosciences, Gould-Simpson Building, University of Arizona, Tuscon, AZ 85721-0077, USA
[7] Rua Esmeralda, 534, Prado, 30410-080 Belo Horizonte, MG, Brazil
[a] Deceased author.

Abstract: Wilancookite, ideally $(Ba,K,Na)_8(Ba,Li,\square)_6Be_{24}P_{24}O_{96}\cdot 32H_2O$, is a new mineral species from the Lavra Ponte do Piauí complex granitic pegmatite, Minas Gerais, Brazil. It occurs as tiny dodecahedral {1 1 0} crystals, deposited on moraesite fibres. Associated primary minerals are albite, montebrasite, Li-bearing micas, cassiterite, elbaite and quartz, while the secondary phosphate association contains fluorapatite, childrenite, eosphorite, zanazziite, greifenstenite, guimarãesite, ushkovite, saléeite and moraesite. The mineral is transparent and colourless, with a vitreous lustre; it is non-fluorescent, brittle, and its streak is white. The estimated Mohs hardness is 4–5, and the calculated density is 3.05 g/cm^3. Wilancookite is isotropic, colourless, non-pleochroic, with $n = 1.560(2)$ (measured under $\lambda = 590$ nm). Electron- and ion-microprobe analyses give (in wt%): P_2O_5 36.19, SiO_2 0.04, Al_2O_3 0.41, BaO 34.65, Na_2O 0.09, K_2O 0.32, BeO 12.86, Li_2O 0.50, and H_2O_{calc} 12.31, total 97.37 wt%. The resulting empirical formula, calculated on the basis of 96 anhydrous oxygen atoms, is $(Ba_{7.54}K_{0.32}Na_{0.14})_{\Sigma 8.00}(Ba_{3.04}Li_{1.57}\square_{1.39})_{\Sigma 6.00}Be_{24.08}(P_{23.88}Al_{0.38}Si_{0.03})_{\Sigma 24.29}O_{96}\cdot 32H_2O$. The single-crystal unit-cell parameters are $a = 13.5398(2)$ Å and $V = 2482.21(7)$ Å^3, space group $I23$. The eight strongest lines in the powder X-ray diffraction pattern [d(in Å)(I)(hkl)] are: 6.90(60)(2 0 0), 5.54(80)(2 1 1), 3.630(60)(3 2 1, 3 1 2), 3.212(70)(3 3 0, 4 1 1), 3.043(100)(4 2 0, 4 0 2), 2.885(70)(3 3 2), 2.774(80)(4 2 2), and 2.398(60)(4 4 0). The crystal structure of wilancookite has been refined, based on single-crystal X-ray diffraction data, to $R_1 = 4.58\%$; the beryllophosphate framework is similar to that occurring in pahasapaite, and is based on zeolite-RHO cages. The mineral species and name were approved by the Commission on New Minerals, Nomenclature and Classification of the International Mineralogical Association (IMA2015-034).

Key-words: wilancookite; new mineral; beryllophosphate; zeolite framework; crystal structure; pegmatite; Minas Gerais; Brazil.

1. Introduction

In Brazil occurs one of the most important pegmatite provinces in the world, the Eastern Brazilian Pegmatite Province (EBPP). This province is located at the East side of the Saõ Francisco craton, mainly in the state of Minas Gerais, but it encompasses also the states of Bahia, Espírito Santo and Rio de Janeiro (de Paiva, 1946; Putzer, 1976; Correia Nevez *et al.*, 1986). Pegmatites from this area are famous for their first-quality gems, but also for mineral systematics since 48 valid mineral species were first described in Minas Gerais (Atencio, 2000, 2008, 2015).

Wilancookite was discovered by Luiz Menezes in 2009, in the Lavra Ponte do Piauí complex granitic pegmatite. The mineral forms colourless tiny dodecahedral crystals, deposited on moraesite fibres. A preliminary examination by energy-dispersive spectrometry showed only Ba and P as major elements; X-ray single-crystal structure determination showed that the mineral was cubic ($a = 13.5398(2)$ Å, space group $I23$), with a beryllophosphate structure topologically identical to that of zeolite-RHO (Nenoff *et al.*, 1996). The presence of Be was then confirmed by SIMS measurements, thus validating the new species.

Wilancookite, ideally $(Ba,K,Na)_8(Ba,Li,\square)_6Be_{24}P_{24}O_{96}\cdot 32H_2O$, was accepted by the Commission on New Minerals, Nomenclature and Classification of the International Mineralogical Association (CNMNC-IMA), under number IMA2015-034. The mineral is named to honour William R. Cook Jr. (1927–2006) and his wife Anne, who accepted to give their name to the mineral. Bill and Anne

DOI: 10.1127/ejm/2017/0029-2661
0935-1221/17/0029-2661 $ 3.60

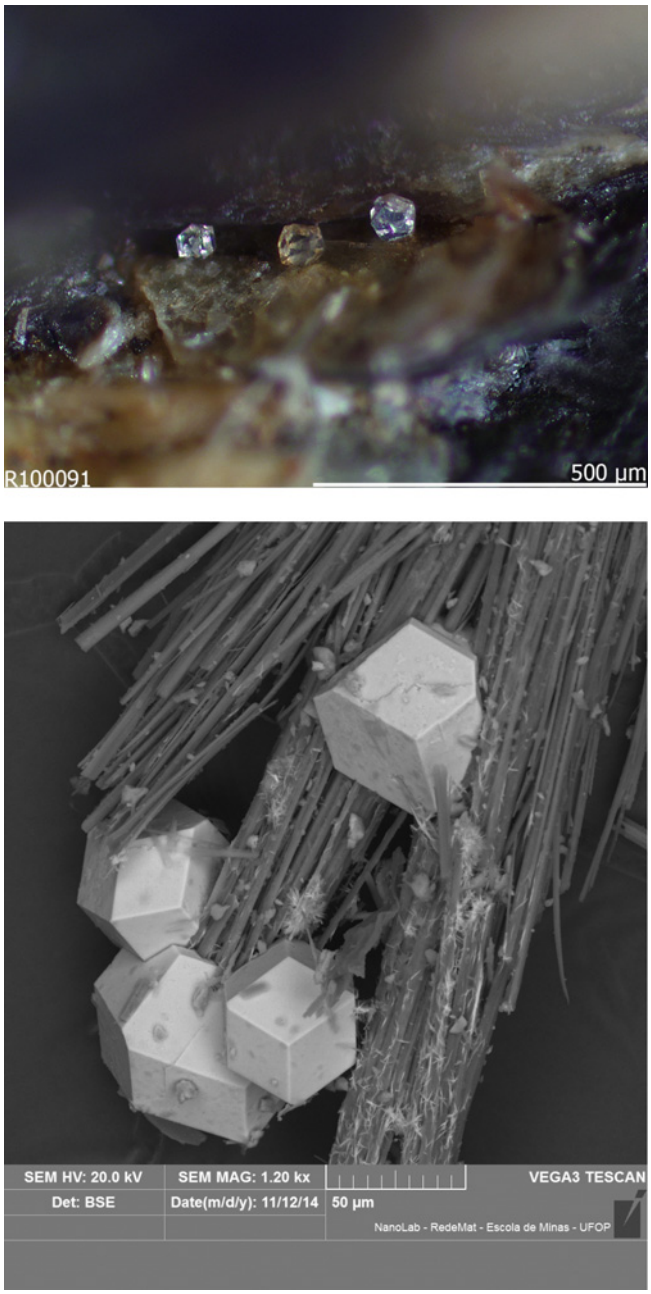

Fig. 1. Dodecahedral crystals of wilancookite, deposited on moraesite fibres. Lavra Ponte do Piauí pegmatite, Minas Gerais, Brazil. (a) Micro-photograph showing the clear colourless crystals; (b) scanning electron microscope image (secondary electrons mode) showing the dodecahedral morphology. (Online version in colour.)

endowed the mineralogy chair at the Cleveland Museum of Natural History; they were founding members of the Mineralogical Society of Cleveland and also of the Micromineral Society of the Cleveland Museum of Natural History. Bill was a mineralogist and crystallographer (BA from Oberlin, MA from Columbia, PhD from Case Western Reserve) (Clifford, 1997). The cotypes are deposited in the collections of the Laboratory of Mineralogy, University of Liège (cotype used for optics, crystal structure and Gandolfi measurements: catalogue number 20394), and in the collections of the Natural History Museum of Luxembourg (cotype used for chemical analyses: catalogue number 2011-33).

2. Occurrence and geological setting

Wilancookite occurs in the Lavra Ponte do Piauí complex granitic pegmatite, Itinga, Jequitinhonha, Minas Gerais, Brazil (16°43′33″ S, 41°53′55″ W). The pegmatite is located in the Araçuaí pegmatite district, one of the subdivisions of the Eastern Brazilian Pegmatite province (Pedrosa-Soares *et al.*, 2011). The pegmatite has been mined for gemstones and samples for the collectors market. It is heterogeneous with well-developed mineralogical and textural zonation (Cassedanne & Philippo, 2015).

The pegmatite is hosted by biotite schist of the Neoproterozoic Salinas Group. The contact is not well exposed and did not allow to determine the orientation of the pegmatite body. A discontinuous quartz core is surrounded by small miarolitic cavities. The primary mineral association is represented by quartz, muscovite, microcline, schorl, and almandine–spessartine (Cassedanne & Philippo, 2015).

Wilancookite is a secondary mineral occurring in phosphate nodules adjacent to the quartz core of the pegmatite. Primary associated minerals are albite, montebrasite, Li-bearing micas, cassiterite, elbaite, and quartz. The secondary phosphate association contains fluorapatite, childrenite, eosphorite, zanazziite, greifenstenite, guimarãesite (Chukanov *et al.*, 2008), ushkovite, saléeite, and moraesite.

The primary phosphate occurring in this pegmatite is montebrasite. Beryllium-rich secondary phosphates formed during late stages, by reaction between montebrasite and beryl. This process produced several species, like beryllonite, greifenstenite, guimarãesite, moraesite, and zanazziite. Wilancookite crystallized in the very late conditions, since the crystals are deposited on moraesite fibres.

3. Physical properties

Wilancookite forms tiny dodecahedral {1 1 0} crystals, deposited on moraesite fibres (Fig. 1). The crystals are transparent, colourless, and reach a diameter of 100 µm. The lustre is vitreous, the streak is white, and the mineral is non-fluorescent under either long or short-wavelength ultraviolet light. No cleavage has been observed, but the mineral is brittle with an irregular fracture. Mohs hardness is 4–5, by analogy with related pahasapaite (see below). The density could not be measured due to small grain size; the calculated density if 3.05 g/cm^3. Wilancookite is isotropic, colourless, non-pleochroic, with $n = 1.560(2)$ (measured under $\lambda = 590$ nm).

4. Chemical composition

Quantitative chemical analyses (Table 1) were performed on isolated crystals with a Cameca SX-50 electron microprobe (Ruhr-Universität Bochum, Germany) oper-

ating in the wavelength-dispersion mode, with an accelerating voltage of 15 kV, a beam current of 10 nA, and a beam diameter of 10 μm. The following standards were used: $AlPO_4$ (P), andradite (Si), spessartine (Al), Ba-glass (Ba), jadeite (Na), and K-glass (K).

The Be and Li contents were determined with a Cameca IMS 4f ion microprobe installed at CNR-IGG, Pavia (Italy). We used a 12.5-kV accelerated $^{16}O^-$ primary-ion beam with a current intensity of 0.7 nA, corresponding to a beam diameter ≤5 μm. The mount was polished, washed in an ultrasonic tank with ethanol, and Pt coated (400 Å thickness) before analysis. Secondary-ion signals of the isotopes $^1H^+$, $^6Li^+$, $^9Be^+$ and $^{31}P^+$ were detected at the electron multiplier. The sample mount, together with the standard mount, was left to degas in the ion-probe sample chamber for a week before analysis under a 2×10^{-9} Torr vacuum. All measurements were done using secondary filtered ions in the range ~75–125 eV (Ottolini *et al.*, 1993, 2002; Hatert *et al.*, 2011) under 25-μm imaged field and the 2^ field aperture (750 μm diameter). Standard used for Li was triphylite from the Buranga pegmatite, Rwanda (Hatert *et al.*, 2011); for Be we selected a sample of natural beryllonite which was previously analyzed by wet colorimetry and atomic absorption spectrophotometry (BeO = 19.70 wt%; P_2O_5 = 55.90 wt%).

The calibration factor for Li in the standard was obtained through the calculation of the experimental Li ion yield having chosen P as the internal reference element for the matrix. We thus derived the ion yield IY (Li/P), defined as $(Li^+/P^+)/((Li(at)/P(at))$ where Li^+ and P^+ are the current intensities detected at the electron multiplier and (at) represents the elemental atomic concentration. It was done similarly for the IY(Be/P) from beryllonite. The two IYs were then used in wilancookite to calculate Li and Be concentrations reported in Table 1. The presence of H, through the $^1H^+$ signal, was confirmed by SIMS analysis but H_2O was not quantified due to the lack of proper calibration standard. The H_2O content of the formula was calculated according to the structural data. CO_2 was not determined but is considered absent according to the structural data.

The empirical formula of wilancookite, based on 96 anhydrous oxygen atoms per formula unit (*apfu*), is: $(Ba_{7.54}K_{0.32}Na_{0.14})_{\Sigma 8.00}(Ba_{3.04}Li_{1.57}\square_{1.39})_{\Sigma 6.00}Be_{24.08}(P_{23.88}Al_{0.38}Si_{0.03})_{\Sigma 24.29}O_{96}\cdot 32H_2O$. The simplified formula is $Ba_8(Ba_3Li_2\square)Be_{24}P_{24}O_{96}\cdot 32H_2O$, which requires P_2O_5 37.06, BeO 13.06, BaO 36.69, Li_2O 0.65, H_2O 12.54, total 100.00 wt%.

5. Raman spectroscopy

The Raman spectrum of wilancookite (Fig. 2) was collected from a randomly oriented crystal at 100% power, on a Thermo Almega Micro-Raman System, using a solid-state laser with a frequency of 532 nm and a thermoelectric cooled CCD detector. The laser was partially polarized with 4 cm^{-1} resolution and a spot size of 1 μm. The spectrum (Fig. 2) is characterized by peaks at 430 (Be–O), 580 (ν_4 PO_4), 1000 (ν_1 PO_4), 1050 (ν_3 PO_4), 1600 (ν_2 H_2O), 3430 and 3680 (ν_3 H_2O) cm^{-1}. Band assignments were established according to the Raman data recently published for strontiohurlbutite, $SrBe_2(PO_4)_2$ (Dal Bo *et al.*, 2014; Rao *et al.*, 2014).

Table 1. Chemical analysis of wilancookite.

Oxide	Mean (wt%)	Range	St. dev.	Cations *pfu***
P_2O_5	36.19	33.39–37.29	1.18	23.88
SiO_2	0.04	0.01–0.07	0.02	0.03
Al_2O_3	0.41	0.27–0.61	0.10	0.38
BaO	34.65	34.07–35.01	0.34	10.58
Na_2O	0.09	0.06–0.13	0.03	0.14
K_2O	0.32	0.26–0.43	0.06	0.32
BeO	12.86	–	0.09	24.08
Li_2O	0.50	–	0.01	1.57
H_2O*	12.31	–	–	64.00
Total	97.37	93.86–98.59	1.41	

* Calculated according to the structural data.
** On the basis of 96 anhydrous oxygen atoms.
Ca and Sr are below detection limits.

6. X-ray structure determination

The powder X-ray diffraction pattern of wilancookite, given in Table 2, was obtained with a Gandolfi camera (diameter 114.6 mm, exposure time 125 h) mounted on a PHILIPS PW-1730/10 X-ray generator using Ni-filtered Cu*K*α radiation (λ = 1.5418 Å). On the basis of the *d*-spacings shown in Table 2, and using the indexation obtained from the structural data, the least-squares refinement program LCLSQ 8.4 (Burnham, 1991) has served to calculate the unit-cell parameters of wilancookite: a = 13.579(9) Å, and V = 2504(5) $Å^3$. The intensities, observed on the Gandolfi film, are in fairly good agreement with those calculated from the structural data (Table 2).

Single-crystal X-ray studies were carried out on an Rigaku Xcalibur 4-circle diffractometer (Mo*K*α radiation, λ = 0.71073 Å), equipped with an EOS detector. A single crystal of wilancookite measuring 0.089 mm × 0.070 mm × 0.065 mm was mounted on a fibreglass; 49 frames with a spatial resolution of 1° were collected by the ϕ/ω scan technique, with a counting time of 700 s/frame, in the range $4.28° < 2\theta < 57.14°$. A total of 1292 reflections were extracted from these frames, corresponding to 805 unique reflections. The unit-cell parameters refined from these reflections, a = 13.5398(2) Å and V = 2482.21(7) $Å^3$, are in good agreement with those refined from the X-ray powder data (see above). Data were corrected for Lorentz, polarization and absorption effects, the latter with an empirical method using the SCALE3 ABSPACK scaling algorithm included in the CrysAlisRED package (Agilent Technologies, 2012).

The crystal structure of wilancookite (Fig. 3) was refined in space group *I*23. Scattering curves for neutral atoms, together with anomalous dispersion corrections,

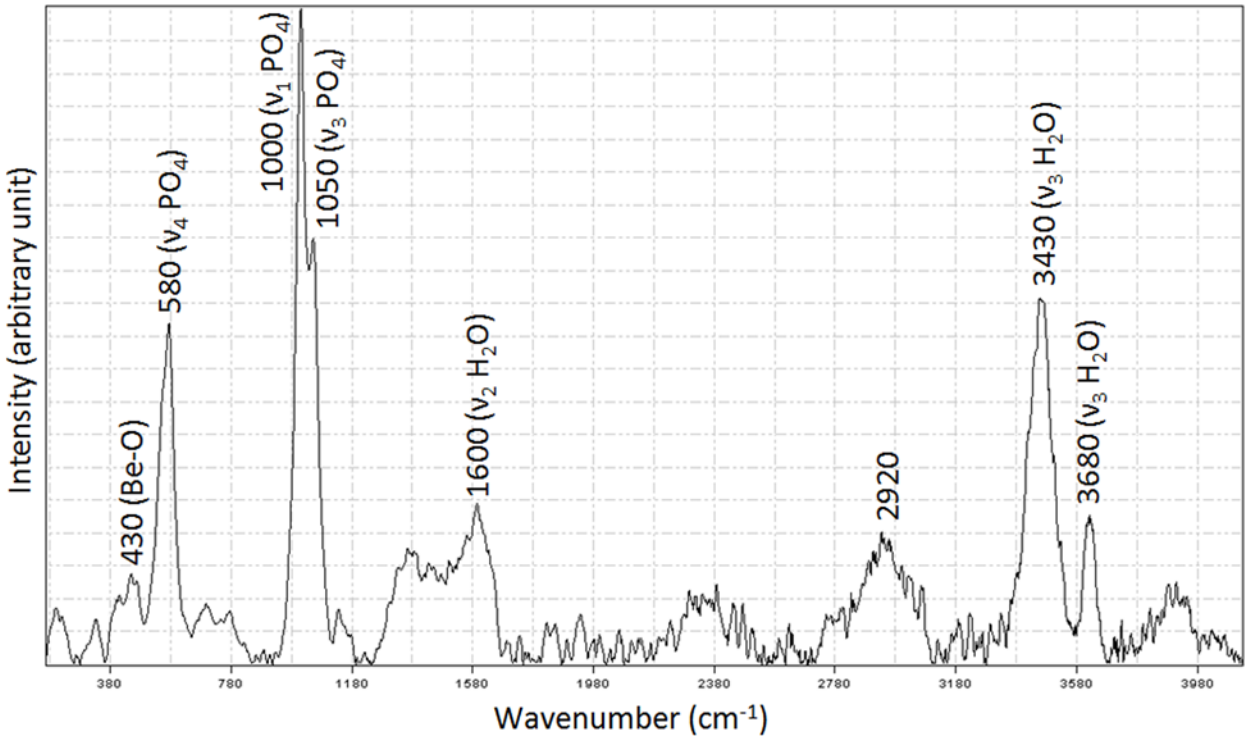

Fig. 2. The Raman spectrum of wilancookite.

Table 2. X-ray powder diffraction pattern of wilancookite.

$I_{obs.}$	$d_{obs.}$	$I_{calc.}$	$d_{calc.}$	*hkl*
10	9.77	63	9.602	1 1 0
60	**6.90**	**60**	**6.790**	**2 0 0**
80	**5.54**	**53**	**5.544**	**2 1 1**
5	4.84	13	4.801	2 2 0
40	4.53	–	–	–
–	–	33	4.294	3 0 1, 3 1 0
30	3.973	30	3.920	2 2 2
60	**3.630**	**45**	**3.629**	**3 2 1, 3 1 2**
20	3.351	1	3.395	4 0 0
70	**3.212**	**66**	**3.201**	**3 3 0, 4 1 1**
100	**3.043**	**100**	**3.036**	**4 2 0, 4 0 2**
70	**2.885**	**60**	**2.895**	**3 3 2**
80	**2.774**	**77**	**2.772**	**4 2 2**
–	–	15	2.663	4 3 1, 5 0 1, 5 1 0, 4 1 3
30	2.485	32	2.479	5 1 2, 5 2 1
60	**2.398**	**38**	**2.401**	**4 4 0**
–	–	6	2.329	5 0 3, 5 3 0, 4 3 3
50	2.262	26	2.263	6 0 0, 4 4 2
40	2.196	30	2.203	6 1 1, 5 2 3, 5 3 2
50	2.148	38	2.147	6 0 2, 6 2 0
–	–	5	2.095	5 1 4, 5 4 1
20	2.052	28	2.047	6 2 2
20	1.999	13	2.002	6 3 1, 6 1 3

Data collected with a Gandolfi camera (diameter 114.6 mm), Cu$K\alpha$ radiation ($\lambda = 1.5418$ Å) filtered with Ni. Intensities were estimated visually. The eight strongest lines are in bold. Calculated intensities were calculated from the structural data with POWDER CELL (Krauz & Nolze, 1996). Calculated *d* values were refined with LCLSQ (Burnham, 1991); the refined *a* value is 13.579(9) Å (space group *I*23).

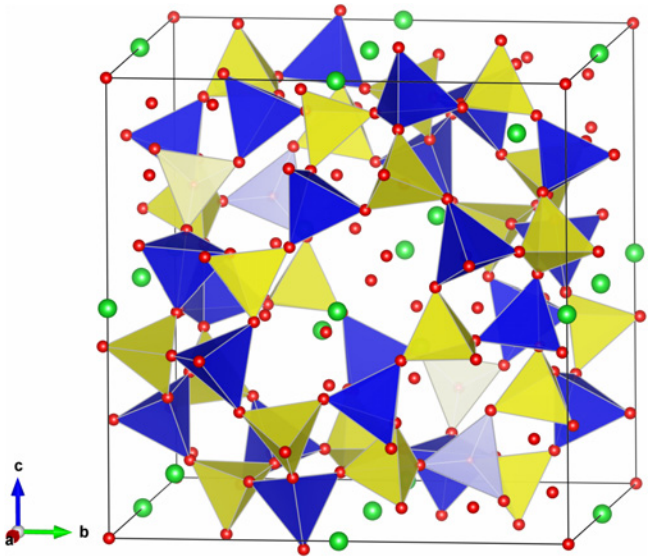

Fig. 3. The crystal structure of wilancookite. The PO_4 tetrahedra are yellow, and the BeO_4 tetrahedra are blue. Green circles represent Ba atoms, and red circles O atoms and water molecules. (Online version in colour.)

were taken from the International Tables for X-ray Crystallography, Vol. C (Wilson, 1992). In the final refinement cycle, all atoms were refined anisotropically, leading to the R_1 value 0.0458. Further details on the crystal structure determination and refinement are given in Table 3; atomic coordinates, anisotropic displacement parameters, and bond lengths and angles are given in Tables 4–6, respectively.

Table 3. Experimental details for the single-crystal X-ray diffraction study of wilancookite.

Dimensions of the crystal (mm)	*ca.* 0.089 × 0.070 × 0.065
a (Å)	13.5398(2)
V (Å^3)	2482.21(7)
Space group	$I23$
Diffractometer	Rigaku XCalibur, EOS detector
Operating conditions	40 kV, 40 mA
Radiation	Mo$K\alpha$ ($\lambda = 0.71073$ Å)
Scan mode	ϕ/ω scan
$2\theta_{min}/2\theta_{max}$	4.28°/57.14°
Range of indices	$-7 \le h \le 17$, $-18 \le k \le 8$, $-9 \le l \le 10$
Measured intensities	1292
Unique reflections	805
Independent non-zero reflections	761 [$F_o > 4\sigma(F_o)$]
Absorption correction	SCALE3 ABSPACK (Agilent Technologies, 2012)
Structure solution program	SHELXS (Sheldrick, 2008)
L.s. refinement program	SHELXL (Sheldrick, 2008)
Refined parameters	73
R_1 ($F_o > 4\sigma(F_o)$)	0.0438
R_1 (all)	0.0458
wR_2 (all)	0.1357
S (goodness of fit)	1.149
Max Δ/σ in the last l.s. cycle	0.000
Max peak and hole in the final ΔF map (e/Å^3)	+1.17 and −0.65

Site occupancy factors (Table 4) indicate that the Ba1 site is nearly fully occupied by Ba, while the Ba2 site contains significant amounts of vacancies. This indicates that the significant amounts of Li, measured with the SIMS technique (see above), also certainly occur on the Ba2 site.

The compatibility index of wilancookite was calculated with the relationship proposed by Mandarino (1981). The calculation of K_P was performed with the calculated density of 3.05 g/cm^3. The compatibility index, $1 - (K_P/K_C)$, is 0.042, and ranges in the category "good" according to Mandarino (1981).

7. Discussion

The crystal structure of wilancookite is characterized by a framework similar to that of pahasapaite, $(Ca,Li,K,\square)_{24}Li_8Be_{24}P_{24}O_{96}\cdot 38H_2O$ (Rouse *et al.*, 1987, 1989). This framework is based on corner-sharing BeO_4 and PO_4 tetrahedra forming a large cavity in which occur Ba atoms and water molecules. As shown in Fig. 3, three different types of rings are building the cavity: eight-membered rings are parallel to (1 0 0) planes, six-membered rings are parallel to (1 1 1) planes, and four-membered rings are parallel to (1 1 0) planes. The positions of Ba atoms and water molecules are significantly different from those of Ca and Li in pahasapaite; however, the general topology of the framework is preserved.

Table 4. Final fractional coordinates and equivalent isotropic displacement parameters (Å^2) for wilancookite.

Site	x	y	z	$U_{eq.}$
Ba1*	0	0.5	0.5	0.0270(4)
Ba2**	0.62566(7)	0.62566(7)	0.37434(7)	0.0323(6)
P	0.8751(2)	0.7219(1)	0.4302(1)	0.0158(5)
Be	0.9303(7)	0.7729(8)	0.6245(8)	0.019(2)
O1	0.8829(4)	0.6206(5)	0.3789(4)	0.022(1)
O2	0.8904(5)	0.6977(4)	0.5401(4)	0.021(1)
O3	0.7724(4)	0.7658(4)	0.4099(4)	0.018(1)
O4	0.9534(4)	0.7947(4)	0.3933(4)	0.020(1)
W1	0.434(1)	0.583(1)	0.282(1)	0.133(7)
W2	0.5	0.5	0.5	0.052(7)

Occupancy factors: *0.967(8) Ba + 0.033(8) □; **0.532(6) Ba + 0.468(6) □.

The beryllophosphate tetrahedral framework of wilancookite is built by an array of truncated cubo-octahedral cages, linked together through octagonal prisms. In zeolite-RHO, the framework is undistorted, while in pahasapaite and wilancookite, both cages and octagonal prisms are strongly distorted (Fig. 4), thus leading to a symmetry reduction from $Im3m$ to $I23$. This symmetry reduction is induced by the ordered distribution of Be and P on the tetrahedral sites of pahasapaite and wilancookite, while Al and Si are completely disordered on a single tetrahedral position in zeolite-RHO (Nenoff *et al.*, 1996; Rouse *et al.*, 1989).

The non-framework species in wilancookite are the Ba1 and Ba2 cations, as well as the W1 and W2 water molecules. These species are located in the cages, on different positions from those found in pahasapaite. The Ba1 atom is coordinated by twelve oxygens, with four short Ba1–O1 bonds of 2.807 Å, and eight long Ba1–O2 and Ba1–O4 bonds of 3.109–3.196 Å, respectively (Table 6). The Ba2 site is coordinated by three O3 atoms located at 2.790 Å, as well as by seven W1 and W2 water molecules located between 2.94 and 3.19 Å (Table 6). The morphologies of the Ba1 and Ba2 sites are compared in Fig. 5, where it appears that the Ba1 site corresponds to a fairly regular hexagonal prism, similar to that observed in minjiangite (Rao *et al.*, 2015), whereas the Ba2 site is more irregular. Cationic distributions on these sites were calculated to reach a good agreement between the site scattering values given by the structure refinement (Table 4), and the chemical composition determined by electron microprobe (Table 1). According to these calculations, the Ba1 site is fully occupied by 94 at% Ba, 4 at% K and 2 at% Na, while the Ba2 site contains 52 at% Ba, 26 at% Li, and 22% vacancies.

The presence of Li on the Ba2 site affects its coordination polyhedron, which becomes more distorted, compared to the coordination polyhedron of the Ba1 site (Fig. 5). Moreover, the average Ba2–O bond distance (2.971 Å) is significantly shorter than the average Ba1–O bond distance (3.037 Å; Table 6), thus confirming the occurrence of Li on the Ba2 site. Lithium generally occurs in tetrahedral or octahedral coordinations (Wenger &

Table 5. Anisotropic displacement parameters (Å^2) for wilancookite.

Site	U_{11}	U_{22}	U_{33}	U_{23}	U_{13}	U_{12}
Ba1	0.0431(6)	0.0161(5)	0.0218(5)	0.000	0.000	0.000
Ba2	0.0323(6)	0.0323(6)	0.0323(6)	0.0045(4)	0.0045(4)	−0.0045(4)
P	0.0139(9)	0.0171(9)	0.0164(9)	−0.0020(7)	0.0000(7)	0.0006(7)
Be	0.015(4)	0.025(5)	0.017(4)	−0.004(4)	0.000(4)	0.001(4)
O1	0.026(3)	0.021(2)	0.020(2)	−0.004(2)	−0.004(2)	0.003(2)
O2	0.027(3)	0.021(3)	0.016(2)	0.001(2)	0.000(2)	−0.009(2)
O3	0.011(2)	0.015(3)	0.029(3)	−0.001(2)	0.002(2)	−0.004(2)
O4	0.014(2)	0.023(3)	0.022(3)	0.001(2)	0.000(2)	0.001(2)
W1	0.15(2)	0.16(2)	0.085(9)	0.04(1)	−0.06(1)	−0.06(1)
W2	0.052(7)	0.052(7)	0.052(7)	0.000	0.000	0.000

Table 6. Selected bond distances (Å) and angles (°) for wilancookite.

P–O1	1.542(5)	Ba1–O1 × 4	2.805(7)
P–O2	1.536(6)	Ba1–O2 × 4	3.109(6)
P–O3	1.537(6)	Ba1–O4 × 4	3.196(6)
P–O4	1.531(6)	Mean	**3.037**
Mean	**1.541**		
Be–O1	1.595(12)	Ba2–O3 × 3	2.790(5)
Be–O2	1.623(11)	Ba2–W1 × 3	2.94(2)
Be–O3	1.630(12)	Ba2–W2	2.947(2)
Be–O4	1.621(11)	Ba2–W1′ × 3	3.19(2)
Mean	**1.617**	Mean	**2.971**
O2–P–O1	103.7(3)	O1–Be–O2	112.1(7)
O2–P–O3	112.2(4)	O1–Be–O4	104.3(7)
O3–P–O1	109.0(3)	O2–Be–O3	110.4(7)
O4–P–O1	112.2(3)	O1–Be–O3	108.9(6)
O4–P–O2	111.1(3)	O4–Be–O2	109.4(7)
O4–P–O3	108.6(3)	O4–Be–O3	111.7(7)
Mean	**109.5**	Mean	**109.5**

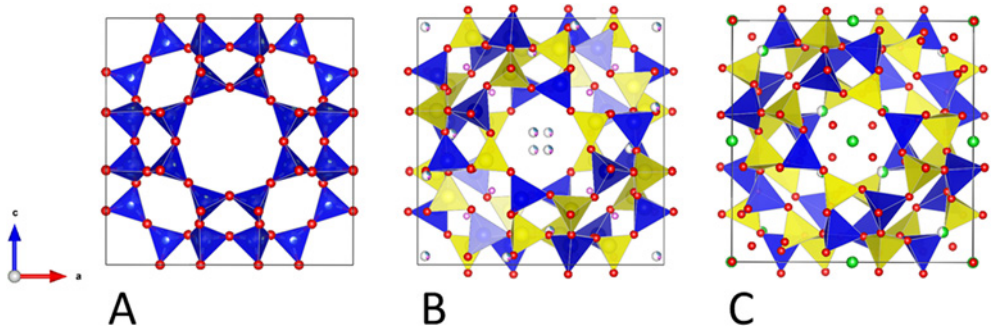

Fig. 4. Comparison of the tetrahedral framework in zeolite-RHO (A – McCusker, 1984), in pahasapaite (B – Rouse *et al.*, 1987), and in wilancookite (C – this work). (Online version in colour.)

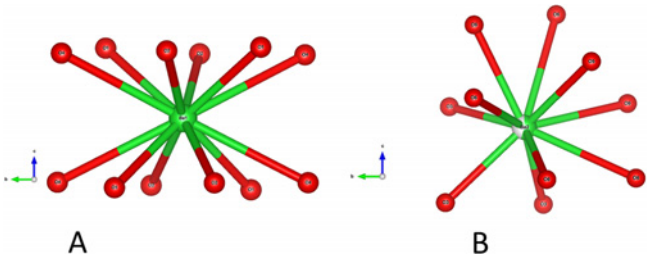

Fig. 5. Morphologies of the Ba1 (A) and Ba2 (B) sites of wilancookite. (Online version in colour.)

Armbruster, 1991); however, the presence of Li on larger crystallographic sites has been extensively demonstrated in synthetic alluaudite-type phosphates (Hatert *et al.*, 2000, 2002; Hatert, 2004; Trad *et al.*, 2010).

Wilancookite belongs to the pahasapaite group, Strunz 8.CA.25, Dana 40.5.7.1.; a comparison of the physical properties of wilancookite and pahasapaite is shown in Table 7. Wilancookite is only the second barium beryllophosphate reported to date, the first one being minjiangite (Rao *et al.*, 2015), a phyllophosphate characterized by a completely different structure topology.

Table 7. Comparison of the physical properties of wilancookite and pahasapaite.

Phase	Wilancookite	Pahasapaite
Reference	This work	[1]
Ideal formula	$(Ba,K,Na)_8(Ba,Li,\square)_6Be_{24}P_{24}O_{96}\cdot 32H_2O$	$(Ca,Li,K,\square)_{24}Li_8Be_{24}P_{24}O_{96}\cdot 38H_2O$
Space group	*I*23	*I*23
a (Å)	13.5398(2)	13.781(4)
Z	1	1
Strong X-ray lines	9.77(10)	9.60(100)
	6.90(60)	–
	5.54(80)	5.61(30)
	–	4.35(40)
	3.630(60)	3.684(90)
	3.212(70)	3.248(90)
	3.043(100)	3.081(30)
	2.885(70)	2.935(90)
	2.774(80)	2.702(60)
	2.398(60)	2.361(10)
Cleavage	None	None
Density	3.05 (calc.)	2.28
N	1.560(2)	1.523(2)
Hardness	4–5	4.5
Colour	Colourless	Colourless to light pink

[1] Rouse *et al.* (1987).

Wilancookite and pahasapaite are the only known phosphate minerals with a zeolite-type topology; however, synthetic beryllophosphates, zincophosphates and zincoarsenates with a zeolite topology were reported by Harvey (1988), Harvey & Meier (1989), Gier & Stucky (1991), and Harrison *et al.* (1991). Other zeolite minerals show a framework based on truncated cubo-octahedral cages connected by channels, as for example paulingite-Ca, $(Ca,K,Na,Ba,\square)_{10}(Si,Al)_{42}O_{84}\cdot 34H_2O$ (Lengauer *et al.*, 1997), and ashcroftine-(Y), $K_5Na_5Y_{12}Si_{28}O_{70}(OH)_2(CO_3)_8\cdot 8H_2O$ (Moore *et al.*, 1987).

Acknowledgements: Many thanks are due to referees for their constructive comments, as well as to the "Fonds National de la Recherche Scientifique", Belgium, for a FRIA PhD grant (No. 93482). R. Scholz thanks CNPq, FAPEMIG and PROPP/UFOP (respectively Grant Nos. 305284/2015-0, APQ-01448-15 and PROPP 09/2016). M. Chaves thanks CNPq (Grant No. 305492/2013-6).

References

Agilent Technologies. (2012): CrysAlis CCD and CrysAlis RED. Oxford Diffraction Ltd, Yarnton, Oxfordshire, UK.

Atencio, D. (2000): Type mineralogy of Brazil. Universidade de São Paulo, Brazil, 114 p.

— (2008): 21st-century Brazilian minerals. *in* "Mineralogy and Museums 6th Conf., Abstract Book", 12.

— (2015): The discovery of new mineral species and type minerals from Brazil. *Braz. J. Geol.*, **45**, 143–158.

Burnham, C.W. (1991): LCLSQ version 8.4, least-squares refinement of crystallographic lattice parameters. Department of Earth & Planetary Sciences, Harvard University, Cambridge, MA, 24 p.

Cassedanne, J. & Philippo, S. (2015): Minerals and gems deposits of the eastern Brazilian pegmatites. Ed. MnhnL, Luxembourg, 674 p.

Chukanov, N.V., Atencio, D., Zadov, A.E., Menezes Filho, L.A.D., Coutinho, J.M.V. (2008): Guimarãesite, a new Zn-dominant monoclinic roscherite-group mineral from Itinga Minas Gerais, Brazil. *New Data Miner.*, **42**, 11–15.

Clifford, J. (1997): William R. Cook Jr. (1927–2006). *Rocks Miner.*, **82**, 257–258.

Correia Nevez, J.M., Pedrosa Soares, A.C., Marciano, V.R.P.d.R.O. (1986): A provincial pegmatítica oriental do Brazil à luz dos conhecimentos atuais. *Rev. Bras. Geociênc.*, **16**, 106–118.

Dal Bo, F., Hatert, F., Baijot, M. (2014): Crystal chemistry of synthetic $M^{2+}Be_2P_2O_8$ (M^{2+} = Ca, Sr, Pb, Ba) beryllophosphates. *Can. Mineral.*, **52**, 337–350.

de Paiva, G. (1946): Província pegmatíticas do Brazil. *Boletim DNPM-DFMP*, **78**, 13–21.

Gier, T.E. & Stucky, G.D. (1991): Low-temperature synthesis of hydrated zinco(beryllo)-phosphate and arsenate molecular sieves. *Nature*, **349**, 508–510.

Harrison, W.T.A., Gier, T.E., Stucky, G.D. (1991): Synthesis and crystal structure of a novel beryllium phosphate open-framework structure. *J. Mater. Chem.*, **1**, 153–154.

Harvey, G. (1988): The synthesis and structure of beryllophosphate-H: a new open-framework zeolite. *Z. Krist.*, **182**, 123–124.

Harvey, G. & Meier, W. (1989): The synthesis of beryllophosphate zeolites. *in* "Zeolites: facts, figures, future. Studies in surface science & catalysis", P.A. Jacobs & R.A. van Santen, eds. Elsevier, Amsterdam, **49**, 411–420.

Hatert, F. (2004): The crystal chemistry of lithium in the alluaudite structure: a study of the $(Na_{1-x}Li_x)_{1.5}Mn_{1.5}Fe^{3+}_{1.5}(PO_4)_3$ solid solution (x = 0 to 1). *Mineral. Petrol.*, **81**, 205–217.

Hatert, F., Keller, P., Lissner, F., Antenucci, D., Fransolet, A.-M. (2000): First experimental evidence of alluaudite-like phosphates with high Li-content: the $(Na_{1-x}Li_x)MnFe_2(PO_4)_3$ series (x = 0 to 1). *Eur. J. Mineral.*, **12**, 847–857.

Hatert, F., Antenucci, D., Fransolet, A.-M., Liegeois-Duyckaerts, M. (2002): The crystal chemistry of lithium in the alluaudite structure: a study of the $(Na_{1-x}Li_x)CdIn_2(PO_4)_3$ solid solution (x = 0 to 1). *J. Solid State Chem.*, **163**, 194–201.

Hatert, F., Ottolini, L., Schmid-Beurmann, P. (2011): Experimental investigation of the alluaudite + triphylite assemblage, and development of the Na-in-triphylite geothermometer: applications to natural pegmatite phosphates. *Contrib. Mineral. Petrol.*, **161**, 531–546.

Krauz, W. & Nolze, G. (1996): POWDER CELL – a program for the representation and manipulation of crystal structures and calculation of the resulting X-ray powder patterns. *J. Appl. Crystallogr.*, **29**, 301–303.

Lengauer, C.L., Giester, G., Tillmanns, E. (1997): Mineralogical characterization of paulingite from Vinaricka Hora, Czech Republic. *Mineral. Mag.*, **61**, 591–606.

Mandarino, J.A. (1981): The Gladstone–Dale relationship: part IV. The compatibility concept and its application. *Can. Mineral.*, **19**, 441–450.

McCusker, L.B. (1984): Crystal structures of the ammonium and hydrogen forms of zeolite RHO. *Zeolites*, **4**, 51–55.

Moore, P.B., Sen Gupta, P.K., Schlemper, E.O., Merlino, S. (1987): Ashcroftine, $Na_{10}(Y,Ca)_{24}(OH)_4(CO_3)_{16}(Si_{56}O_{140})\cdot 16H_2O$, a structure with enormous polyanions. *Am. Mineral.*, **72**, 1176–1189.

Nenoff, T.M., Parise, J.B., Jones, G.A., Galya, L.G., Corbin, D.R., Stucky, G.D. (1996): Flexibility of the zeolite-RHO framework. In situ X-ray and neutron powder structural characterization of cation-exchanged BePO and BeAsO RHO analogs. *J. Phys. Chem.*, **100**, 14256–14264.

Ottolini, L., Bottazzi, P., Vannucci, R. (1993): Quantification of lithium, beryllium and boron in silicates by secondary ion mass spectrometry using conventional energy filtering. *Anal. Chem.*, **65**, 1960–1968.

Ottolini, L., Camara, F., Hawthorne, F.C., Stirling, J. (2002): SIMS matrix effects in the analysis of light elements in silicate minerals: comparison with SREF and EMPA data. *Am. Mineral.*, **87**, 1477–1485.

Pedrosa-Soares, A.C., De Campos, C.M., Noce, C.M., da Silva, L.C., Novo, T.A., Roncato, J., Medeiros, S.M., Castañeda, C., Queiroga, G.N., Dantas, E., Dussin, I.A., Alkmim, F. (2011): Late Neoproterozoic-Cambrian granitic magmatism in Araçuaí orogen (Brazil), the Eastern Brazilian Pegmatite Province and related mineral resources. *Geol. Soc. Spec. Publ.*, **350**, 25–51.

Putzer, H. (1976): Metallogenetische Provinzen in Südamerika. Schweizerbart'sche Verlagsbuchhandlung, Stuttgart, 316 p.

Rao, C., Wang, R., Hatert, F., Gu, X., Ottolini, L., Hu, H., Dong, C., Dal Bo, F., Baijot, M. (2014): Strontiohurlbutite, $SrBe_2(PO_4)_2$, a new mineral from Nanping no. 31 pegmatite, Fujian Province, Southeastern China. *Am. Mineral.*, **99**, 494–499.

Rao, C., Hatert, F., Wang, R.C., Gu, X.P., Dal Bo, F., Dong, C.W. (2015): Minjiangite, $BaBe_2(PO_4)_2$, a new mineral from Nanping No. 31 pegmatite, Fujian province, Southeastern China. *Mineral. Mag.*, **79**, 1195–1202.

Rouse, R.C., Peacor, D.R., Dunn, P.J., Campbell, T.J., Roberts, W.L., Wicks, F.J., Newbury, D. (1987): Pahasapaite, a beryllophosphate zeolite related to synthetic zeolite RHO, from the Tip Top pegmatite of South Dakota. *N. Jb. Mineral. Mh.*, **1987**, 433–440.

Rouse, R.C., Peacor, D.R., Merlino, S. (1989): Crystal structure of pahasapaite, a beryllophosphate mineral with a distorted zeolite RHO framework. *Am. Mineral.*, **74**, 1195–1202.

Sheldrick, G.M. (2008): A short history of SHELX. *Acta Crystallogr.*, **A64**, 112–122.

Trad, K., Carlier, D., Croguennec, L., Wattiaux, A., Ben Amara, M., Delmas, C. (2010): Structural study of the $Li_{0.5}Na_{0.5}MnFe_2(PO_4)_3$ and $Li_{0.75}Na_{0.25}MnFe_2(PO_4)_3$ alluaudite phases and their electrochemical properties as positive electrodes in lithium batteries. *Inorg. Chem.*, **49**, 10378–10389.

Wenger, M. & Armbruster, T. (1991): Crystal chemistry of lithium: oxygen coordination and bonding. *Eur. J. Mineral.*, **3**, 387–399.

Wilson, A.J.C. (1992): International Tables for X-ray Crystallography, Vol. C. Kluwer Academic Press, London, 883 p.

Received 16 December 2016
Modified version received 27 April 2017
Accepted 10 May 2017